AIP | Journal of Applied Physics

Probing the effect of point defects on the leakage blocking capability of Al0.1Ga0.9N/Si structures using a monoenergetic positron beam

Akira Uedono, Ming Zhao, and Eddy Simoen

Citation: Journal of Applied Physics **120**, 215702 (2016); doi: 10.1063/1.4970984
View online: http://dx.doi.org/10.1063/1.4970984
View Table of Contents: http://scitation.aip.org/content/aip/journal/jap/120/21?ver=pdfcov
Published by the AIP Publishing

Probing the effect of point defects on the leakage blocking capability of $Al_{0.1}Ga_{0.9}N$/Si structures using a monoenergetic positron beam

Akira Uedono,[1] Ming Zhao,[2] and Eddy Simoen[2,3]
[1]*Division of Applied Physics, Faculty of Pure and Applied Science, University of Tsukuba, Tsukuba, Ibaraki 305-8573, Japan*
[2]*Imec, Kapeldreef 75, B-3001 Heverlee, Leuven, Belgium*
[3]*Department of Solid-State Sciences, Ghent University, Krijgslaan 281 S1, 9000 Gent, Belgium*

(Received 17 September 2016; accepted 16 November 2016; published online 2 December 2016)

Vacancy-type defects in $Al_{0.1}Ga_{0.9}N$ were probed using a monoenergetic positron beam. $Al_{0.1}Ga_{0.9}N$ layers with different carbon doping concentrations ($[C] = 5 \times 10^{17} - 8 \times 10^{19}\,cm^{-3}$) were grown on Si substrates by metalorganic vapor phase epitaxy. The major defect species in $Al_{0.1}Ga_{0.9}N$ was determined to be a cation vacancy (or cation vacancies) coupled with nitrogen vacancies and/or with carbon atoms at nitrogen sites (C_Ns). The charge state of the vacancies was positive because of the electron transfer from the defects to C_N-related acceptors. The defect charge state was changed from positive to neutral when the sample was illuminated with photon energy above 1.8 eV, and this energy range agreed with the yellow and blue luminescence. For the sample with high [C], the charge transition of the vacancies under illumination was found to be suppressed, which was attributed to the trapping of emitted electrons by C_N-related acceptors. With increasing [C], the breakdown voltage under the reverse bias condition increased. This was explained by the trapping of the injected electrons by the positively charged vacancies and C_N-related acceptors. *Published by AIP Publishing.* [http://dx.doi.org/10.1063/1.4970984]

I. INTRODUCTION

Gallium nitride (GaN) heterojunction transistors have been of great interest for high-voltage and high-frequency electronics.[1,2] The potential of GaN-based devices is mainly attributed to the superior physical properties of GaN, such as its wide bandgap, large breakdown electric field, and high saturation electron velocity. Most GaN-based devices have been fabricated using GaN layers grown on foreign substrates, such as sapphire and SiC, using metalorganic vapor phase epitaxy (MOVPE). Recent developments in the growth techniques used to obtain GaN layers on Si substrates have triggered a substantial upsurge in research activity and significant progress has therefore been made in this field.[3–6] The primary motivation for the development of the GaN-on-Si technology is its low production cost and the availability of large diameter substrates. In addition, further cost benefits are expected if the devices can be processed using tools in standard fabrication plants for Si-based devices.

During the fabrication of GaN-on-Si structures, the large difference between the thermal expansion coefficients of Si and GaN introduces tensile stress in the GaN layers, which might lead to layer cracking. To avoid crack formation, AlGaN buffer layers and/or AlN interlayers can be introduced between GaN and Si. There have been increasing requirements for a buffer layer with enhanced leakage current blocking capabilities. Thus, it is highly demanding to control the electrical resistance of the buffer layers to meet such requirements. An increase in the buffer thickness is a straightforward solution; however, wafer bowing becomes very severe when the buffer thickness exceeds a certain value, causing problems in the device fabrication process.

It is known that incorporating carbon (C) to the AlGaN and GaN layers effectively increases the resistance of these layers.[7–12] According to the density functional theory,[13,14] C in GaN is an amphoteric dopant, and C substituting N (C_N) acts as a deep acceptor. A high concentration of C ($\geq 10^{19}\,cm^{-3}$) is commonly required to obtain highly resistive GaN and AlGaN layers. This suggests that a high concentration of deep traps is generated in the C-doped GaN and AlGaN layers, which play an important role in the suppression of the leakage current. However, high C-doping is expected to simultaneously introduce point and structural defects in these layers and could be related to the formation of leakage paths in GaN and AlGaN layers. Because point defects in GaN and AlGaN also act as electron/hole trap centers, the study of their charge/discharge processes is of high importance in understanding the buffer related dispersion and current collapse issues in power transistors.[15] Despite tremendous research efforts, C-doping related point defect generation, buffer leakage mechanism, and buffer dispersion have by far not been well understood. Positron annihilation is a powerful technique to evaluate vacancy-type defects in semiconductors,[16,17] and defects in group-III nitrides have been successfully investigated using this method.[18–24] In this study, we used a monoenergetic positron beam to probe native vacancies in $Al_{0.1}Ga_{0.9}N$ layers grown on Si substrates. We showed that the obtained results provided additional insights to explain the change in the leakage blocking capability of these layers.

II. EXPERIMENTAL PROCEDURE

The stack investigated in this study consists of $Al_xGa_{1-x}N$ (1.8 μm)/$Al_{0.44}Ga_{0.56}N$ (500 nm)/$Al_{0.75}Ga_{0.25}N$

(500 nm)/AlN (200 nm) (as depicted in the inset of Fig. 3). The growth was carried out on 200 mm Si (111) substrates, using a Veeco TurboDisc MaxBright MOVPE system.[6,25] Trimethylgallium, trimethylaluminum, and ammonia (NH_3) were used as precursors for Ga, Al, and N, respectively. The samples were characterized in-line using X-ray diffraction (XRD) with a QC3 system from Bruker ($CuK\alpha_1$ radiation). The mole fractions of Al, x, in the $Al_xGa_{1-x}N$ layers were determined as 0.1 from the XRD omega-2theta spectra. The carbon concentration [C] in the $Al_{0.1}Ga_{0.9}N$ layers was varied from $5\times10^{17}\,cm^{-3}$ to $8\times10^{19}\,cm^{-3}$ by changing the growth temperature from 1040 °C to 950 °C, where [C] was measured by secondary ion mass spectrometry from reference samples with the same growth conditions. For buffer leakage measurements, square ($100\,\mu m \times 100\,\mu m$) metal dots were deposited on the samples by Ti/Au metallization and lift-off. The leakage current was measured by sweeping the voltage bias supplied to the metal dots, with the silicon substrate grounded. Photoluminescence (PL) spectra were measured using a 325 nm He-Cd laser as an excitation source and a Perkin-Elmer Lambda 950 UV–visible–near infrared spectrophotometer. All measurements were carried out at room temperature.

Details of the positron annihilation technique are described elsewhere.[16,17] In the present experiment, the Doppler broadening spectra of the annihilation radiation as a function of the incident positron energy E were measured using Ge detectors. The spectra were characterized by the S parameter, defined as the fraction of annihilation events over the energy range of 510.2–511.8 keV, and by the W parameter, defined as the fraction of annihilation events in the ranges of 504.2–507.6 keV and 514.4–517.8 keV. Doppler broadening spectra were also measured using a coincidence system. Measurements of the Doppler broadening spectrum were done in the dark and under illumination of a 325 nm He-Cd laser. The laser beam was defocused at the sample position, and the total area of the sample (size: 1 cm × 1 cm) was illuminated with an irradiance of 10 mW/cm^2. The relationship between the S value and the photon energy was measured using a spectrometer with a Xe lamp. The irradiance of the spectrometer depends on the photon energy (0.02–0.2 mW/cm^2), but no relationship between S and the irradiance was observed in the present experiment. The relationship between S and E was analyzed using VEPFIT (Variable Energy Positron FIT), a computer program developed by van Veen *et al.*[26] The application of the VEPFIT code to GaN is described elsewhere.[27]

Doppler broadening spectra corresponding to the annihilation of positrons from the delocalized state in $Al_{0.125}Ga_{0.875}N$ and C_N in GaN were theoretically calculated using a computational code QMAS (Quantum MAterials Simulator),[28] which adopts the projector augmented-wave method[29] and the plane-wave basis. The exchange and correlation energy of electrons were described by the generalized gradient approximation.[30] We used the Boroński-Nieminen enhancement factor and positron-electron correlation energy[31] with a small modification to deal with semiconductors.[32] Further details are described in Ref. 33. Those calculations were performed on an orthorhombic supercell. The supercell dimension was $2\sqrt{3}\ a_0 \times 4\ a_0 \times 2\ c_0$, where $a_0 = 0.3189$ nm and $c_0 = 0.5186$ nm are the lattice parameters of the wurtzite cell. Atomic positions in the fixed cell (with the experimental lattice parameters) were computationally optimized through a series of first-principles electronic-structure calculations. The bulk structure of $Al_{0.125}Ga_{0.875}N$ was generated by means of the special-quasirandom-structure approach.[34] Atomic positions were then optimized by first-principles quenched molecular dynamics. The simulated Doppler broadening spectrum was characterized by S and W. The values of S and W for $Al_{0.1}Ga_{0.9}N$ were obtained by an interpolation between the values for GaN and $Al_{0.125}Ga_{0.875}N$.

III. RESULTS AND DISCUSSION

Figure 1 shows the relationship between leakage current density J and reverse bias voltage V_R for $Al_{0.1}Ga_{0.9}N$ with different carbon concentrations ($[C] = 5\times10^{17}-8\times10^{19}\,cm^{-3}$). For the $Al_{0.1}Ga_{0.9}N$ with $[C] = 5\times10^{17}\,cm^{-3}$, a sudden increase in the leakage occurred at ~35 V with a very steep slope and the leakage current density was then suppressed until ~190 V. Above 200 V, the leakage started to increase again. A similar behavior of the $J-V_R$ relationship was observed for $Al_{0.1}Ga_{0.9}N$ with $[C] = 3\times10^{18}\,cm^{-3}$, but the initial leakage started at ~130 V with a J more than one order of magnitude smaller than that from the $Al_{0.1}Ga_{0.9}N$ with $[C] = 5\times10^{17}\,cm^{-3}$. The further increase of the leakage took place only from ~270 V. With increasing [C] ($\geq 2\times10^{19}\,cm^{-3}$), the initial leakage current at the bias voltage below 200 V was effectively suppressed and the slope of J is much lower for the sample with the highest [C]. An initial leakage increase followed by a suppression at a low reverse bias has been reported previously, and it was attributed to the space-charge-limited current (SCLC) conduction process.[35,36] However, the initial leakage increase slope in our case was too high to be possibly explained by the SCLC model[37,38] or other conduction mechanisms alone. An in-depth investigation on this observation is on-going and the results will be

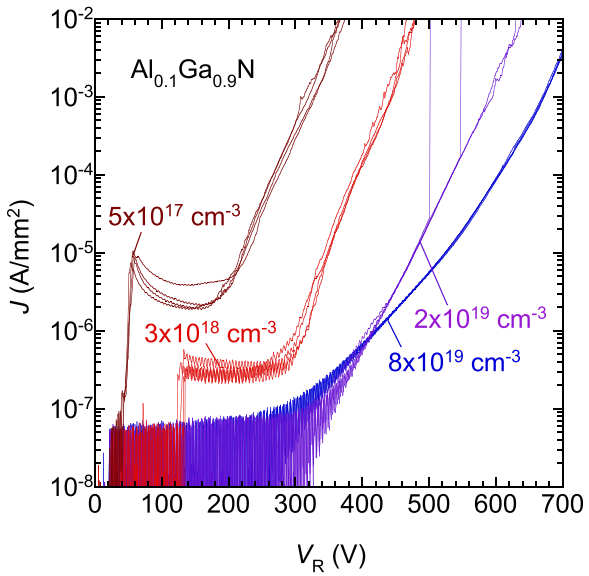

FIG. 1. Current density J and reverse bias voltage V_R characteristics for $Al_{0.1}Ga_{0.9}N$ with different carbon concentrations ($[C] = 5\times10^{17}-8\times10^{19}\,cm^{-3}$).

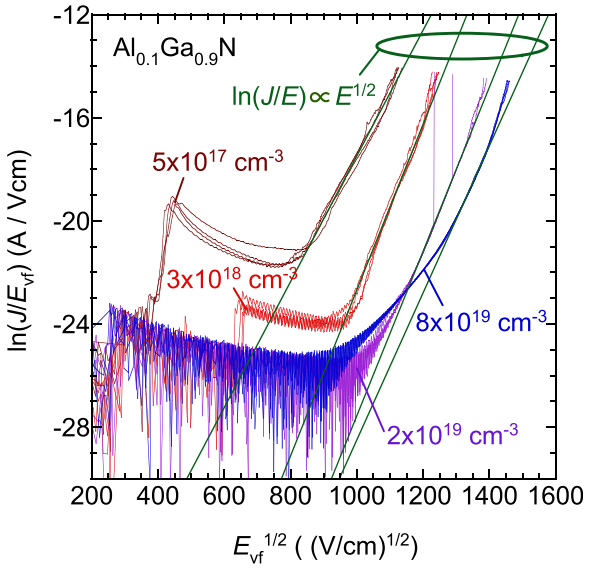

FIG. 2. Relationship between $\ln(J/E_{vf})$ and $E_{vf}^{1/2}$ for $Al_{0.1}Ga_{0.9}N$ with $[C] = 5 \times 10^{17} - 8 \times 10^{19}\,cm^{-3}$.

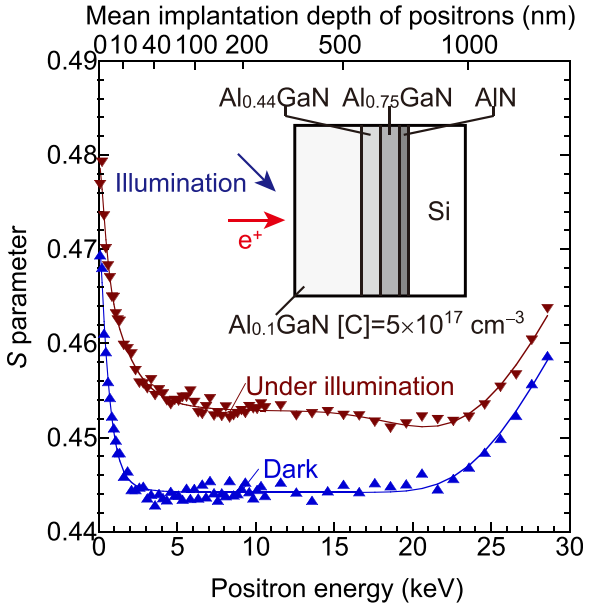

FIG. 3. S parameters as a function of incident positron energy E for $Al_{0.1}Ga_{0.9}N$ with $[C] = 5 \times 10^{17}\,cm^{-3}$. The measurement was done in the dark and under illumination of He-Cd laser light. The inset shows the layer structure of the sample.

published elsewhere. Nevertheless, it is very clear that this initial leakage at low bias voltage is [C] dependent, and a high [C] of $\geq 2 \times 10^{19}\,cm^{-3}$ can completely suppress the initial leakage. In the region of a high reverse bias of >200 V, the leakage seemed to follow the Poole-Frenkel conduction model, evidenced by a linear relation between $\ln(J/E_{vf})$ and $E_{vf}^{1/2}$ (where E_{vf} is the vertical electric field applied to the sample), as shown in Fig. 2. In this figure, lines are results of linear fittings, where fitting regions for the samples with $[C] = 5 \times 10^{17}$, 3×10^{18}, 2×10^{19}, and $8 \times 10^{19}\,cm^{-3}$ are 850–1100, 1050–1200, 1150–1350, and 1300–1400 $(V/cm)^{1/2}$, respectively. A similar observation for the leakage current at a high electric field has been also made by other groups.[39,40] As [C] increases, $\ln(J/E_{vf})$–$E_{vf}^{1/2}$ curves gradually became super-linear, suggesting a gradual deviation from a pure Poole-Frenkel conduction mechanism as increasing [C].

Figure 3 shows the S values of the $Al_{0.1}Ga_{0.9}N$ layer with $[C] = 5 \times 10^{17}\,cm^{-3}$ as a function of incident positron energy E. The mean implantation depth of positrons is shown on the upper horizontal axis. The S value increased with decreasing E (<3 keV), which corresponds to the diffusion of positrons towards the surface. The increase in the S value at $E > 20$ keV is mainly due to the annihilation of positrons in Si. The solid curves shown in Fig. 3 are fitting curves of the experimental data; here, a reasonable agreement between the experimental data and the fitting curves was obtained using the sample structure described in Section II. The diffusion length of positrons, L_d, was obtained to be 5 ± 1 nm for $Al_{0.1}Ga_{0.9}N$ without illumination. The typical value of L_d for defect-free (DF) undoped GaN is reported to be 60–90 nm.[27,41,42] The diffusion length of positrons decreases due to several factors, such as the trapping of positrons by vacancy-type defects and scattering from charged impurities. As discussed later, the S value for $Al_{0.1}Ga_{0.9}N$ measured in the dark was close to that of the positron annihilation from the delocalized state of GaN, suggesting that the trapping fraction of positrons by vacancies is small. The observed short diffusion length is likely to be caused by the scattering/trapping of positrons by charged defects such as positively charged vacancies and C-related defects. We will elaborate this observation in the later part of this section.

As shown in Fig. 3, the S values corresponding to the annihilation of positrons in $Al_{0.1}Ga_{0.9}N$ were increased by illumination of He-Cd laser light. The transition of the charge state of vacancy-type defects (V) from positive to neutral (or neutral to negative), $V^+ \rightarrow V^0$ (or $V^0 \rightarrow V^-$), increases the trapping probability of positrons.[16] Thus, the observed increase in the S value can be attributed to the capture of electrons by vacancy-type defects and a resultant charge transition of the defects.

For $Al_{0.1}Ga_{0.9}N$ with different [C], Doppler broadening spectra were measured using the coincidence system. In these measurements, the value of E was fixed at 10 keV (mean implantation depth of positrons is 200 nm). Figure 4 shows the S–W plot for $Al_{0.1}Ga_{0.9}N$ with and without illumination. The (S,W) value for GaN grown by hydride vapor phase epitaxy (HVPE) is also shown, where the value was measured at $E = 30$ keV. The (S,W) value for HVPE-GaN represents the value for the positron annihilation from the delocalized state in GaN.[27] The (S,W) values for defect free (DF)-GaN, DF-$Al_{0.1}Ga_{0.9}N$, and typical defects in GaN simulated using the QMAS code are also shown.[27,33,43,44] In this figure, a Ga vacancy V_{Ga} (or $(V_{Ga})_2$) coupled with nitrogen vacancies V_Ns, carbon, and oxygen at nitrogen sites is shown as $V_{Ga}(V_N)_m$, $(V_{Ga}V_N)_2$, $V_{Ga}(O_N)_n$, and $V_{Ga}(C_N)_l$, (n, m, l = 1–4), respectively.

When a sample contains vacancy-type defects, positrons may annihilate from the delocalized state and the trapped state of the defects. In this case, the (S,W) value is obtained as a weighted average of the characteristic (S,W) values for those states and should lie on a line connecting them. If the

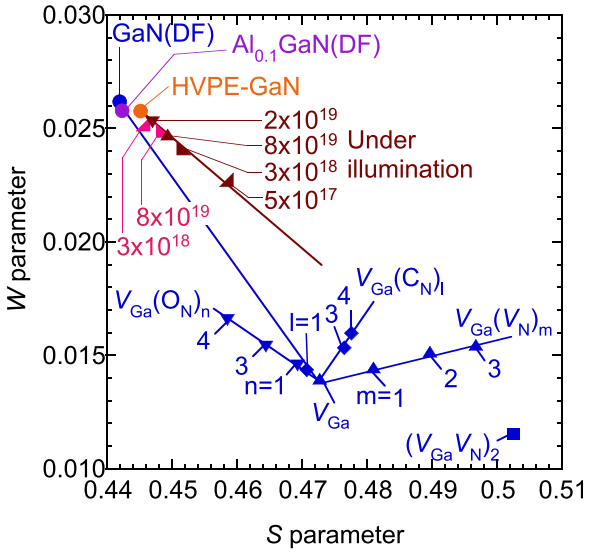

FIG. 4. Relationship between S and W corresponding to the positron annihilation in $Al_{0.1}Ga_{0.9}N$ measured with and without He-Cd laser illumination. The values of [C] in $Al_{0.1}Ga_{0.9}N$ are shown in the figure. The result for HVPE-GaN is also shown. The simulated (S,W) values corresponding to the annihilation of positrons in the delocalized state (DF) and those of positrons trapped by vacancy-type defects in GaN are shown in the same figure.

sample contains more than one defect species, the (S,W) value corresponding to the trapped states of vacancies becomes a weighted average of characteristic values of those defects. As shown in Fig. 4, the difference between the (S,W) values for DF-GaN and DF-$Al_{0.1}Ga_{0.9}N$ is small. Thus, the (S,W) values for cation vacancy (V_{III}) related defects in $Al_{0.1}Ga_{0.9}N$, such as $V_{III}(V_N)_m$, $V_{III}(O_N)_n$, and $V_{III}(C_N)_l$, are expected to be close to the (S,W) values for such defects in GaN. The relationship between the (S,W) values for HVPE-GaN and $Al_{0.1}Ga_{0.9}N$ with $[C] = 3 \times 10^{18}\,cm^{-3}$ (measured in the dark) was close to that of the simulated values for DF-GaN and DF-$Al_{0.1}Ga_{0.9}N$, suggesting that almost all positrons annihilate from the delocalized state. For $Al_{0.1}Ga_{0.9}N$ with different [C], the S values measured under illumination are located on a straight line. This means that the probed defect species in those samples are the same. These (S,W) values are located on the right-hand side of the line that connects the values for DF-GaN and V_{Ga}. Thus, the defect species in $Al_{0.1}Ga_{0.9}N$ is unlikely to be pure V_{III} or V_{III} coupled with O_Ns, but to be vacancy agglomerates such as $V_{III}(V_N)_n$ and $(V_{III}V_N)_2$, or complexes between V_{III}-type defects and C_Ns. The dislocation density of the samples was estimated to be around or less than $1 \times 10^{10}\,cm^{-2}$ according to the planar view transmission electron microscope inspection. The mean distance between dislocations, therefore, can be estimated to be an order of 100 nm. For the present samples, the diffusion length of positrons was obtained to be 5 nm. This short diffusion length suggests that the positrons mainly annihilate in the region where they reached the thermalized condition. Thus, the dislocation is not the major trapping site of positrons in the present samples.

The defect concentration in $Al_{0.1}Ga_{0.9}N$ with $[C] = 5 \times 10^{17}\,cm^{-3}$ was estimated as follows. According to the trapping model of positrons,[16] the observed S value, S_{obs}, is given by $S_{obs} = S_f\,(1 - F_d) + S_d F_d$, where S_f, S_d, and F_d are the S values corresponding to the annihilation of positrons from the free state, which trapped by the defect, and the trapping fraction of positrons by the defect, respectively. The relationship between F_d and the defect concentration C_d is given by $F_d = \mu_d C_d / (\lambda_f + \mu_d C_d)$, where μ_d and λ_f are the trapping rate of positrons and the annihilation rate of positrons from the free-state, respectively. Assuming that the major defect species is $V_{Ga}(V_N)_2$, we use the calculated S value of $V_{Ga}(V_N)_2$ as S_d. This S_d value was normalized by the calculated S value for DF-GaN ($S_d/S_f = 1.108$). The observed S value was normalized by using S for HVPE-GaN (1.031). The typical value of μ_d for a neutral monovacancy is $5 \times 10^{14}\ s^{-1}$.[16] Using λ_f calculated by the PAW method ($6.27 \times 10^9\ s^{-1}$), C_d was estimated to be $4 \times 10^{17}\,cm^{-3}$. When we use S for $V_{Ga}(C_N)_4$ as S_d, its concentration was estimated to be $7 \times 10^{17}\,cm^{-3}$, which is at the same order of magnitude as the [C] for this sample.

Using the averaged value of those estimated [C] ($6 \times 10^{17}\,cm^{-3}$) above and μ_d for a positively charged monovacancy ($3 \times 10^{13}\ s^{-1}$, Ref. 16), S_{obs} for the positively charged defect can be estimated to be 0.447, which reasonably agrees with the S value obtained without illumination (0.4487). Thus, we can conclude that the behavior of S for the samples with and without illumination can be explained by assuming the presence of positively charged V_{III}-type defects in $Al_{0.1}Ga_{0.9}N$. The introduction of the positively charged vacancies can be associated with C_N, which acts as an acceptor ($V^0 + C_N^0 \rightarrow V^+ + C_N^-$). In this case, because C_N does not take an electron from the valence band, it does not contribute an increase in the carrier concentration in $Al_{0.1}Ga_{0.9}N$.

Figure 5 shows the S value for $Al_{0.1}Ga_{0.9}N$ with $[C] = 5 \times 10^{17}\,cm^{-3}$ as a function of the photon energy. During the measurements, E was fixed at 10 keV. The PL spectrum for this sample is also shown. The oscillation in the spectrum is caused by the reflection of the laser light at the front- and backside of the sample. The band gap energy of $Al_{0.1}Ga_{0.9}N$ was calculated to be 3.6 eV using the bowing

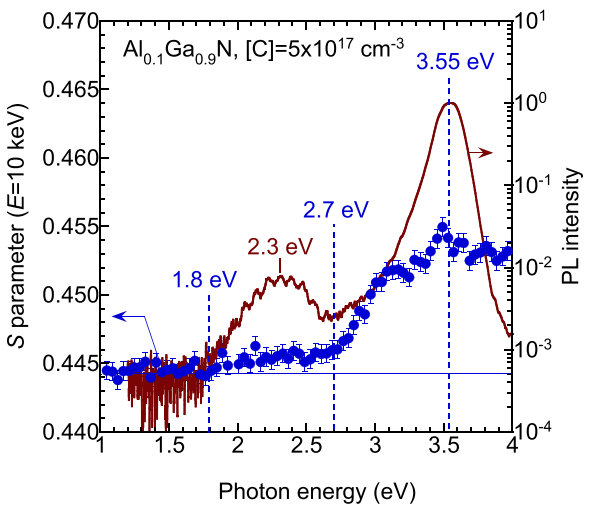

FIG. 5. Relationship between the S value and the photon energy for $Al_{0.1}Ga_{0.9}N$ with $[C] = 5 \times 10^{17}\,cm^{-3}$. During the measurement, the value of E was set to 10 keV. The PL spectrum obtained at room temperature is also shown.

parameter obtained for $Al_xGa_{1-x}N$ $(0 \le x < 0.45)$.[45] Thus, the luminescence peak near 3.55 eV can be attributed to near band edge (NBE) emission. This luminescence band seems to be broadened on the low energy side (2.7–3.5 eV), which is anticipated to be caused by the blue luminescence (BL) band. It was reported that a broad BL band was observed in semi-insulating C-doped GaN, which was attributed to the C-related defects.[46–48] A broad yellow luminescence (YL) band with a maximum at 2.3 eV was also observed. The origin of the YL band has been a subject of debate for a long time. However, it was often attributed to defects such as C_N or $V_{Ga}O_N$.[13,46]

In Fig. 5, the S value increases at a photon energy of 1.8 eV. Above 2.7 eV, a further increase in S was observed, and it saturated at 3.2 eV. The maximum of the S value agreed with NBE. The observed behaviors of S correlated well with the YL and BL bands, suggesting that these emission processes involve the interaction between the vacancy-type defects and electrons excited by illumination. A similar increase of S above a photon energy of 2.7 eV has been reported for unintentionally C-doped GaN.[43,44] Because the bandgap of $Al_{0.1}Ga_{0.9}N$ is larger than that of GaN, the separation between the increases in S at BL band and NBE was clearly observed in the present experiment. The electron capturing by vacancy-type defects can be divided into direct and indirect processes. For example, the electron emitted from the valence band is trapped by the vacancy-type defects (direct process). For the indirect process, the electron is first excited to the energy levels that cause NBE, and then it was captured by the vacancies that have the energy levels lower than those of NBE.

Figure 6(a) shows the full width at half maxima (FWHM) values of $Al_{0.1}Ga_{0.9}N$ (002) and (102) peaks obtained from XRD ω-rocking curves as a function of [C]. It can be seen that the FWHM of both $Al_{0.1}Ga_{0.9}N$ (002) and (102) peaks monotonically increases as increasing [C], indicating a worse crystal quality at a higher [C]. This trend agrees very well with the widely observed behavior in III-N MOVPE and is mainly due to a larger number of structural defects, such as dislocations, impurity clusters, etc., introduced at a lower growth temperature. Figure 6(b) summarizes the leakage blocking capability of the samples. It is represented by the breakdown voltage, $V_{BD(R)}$, which is defined as the voltage at a leakage current of 10 μA/mm^2 under the reverse bias condition. It can be observed that $V_{BD(R)}$ first increases significantly when [C] increases from 5×10^{17} cm^{-3} to 2×10^{19} cm^{-3} and then $V_{BD(R)}$ tends to saturate with further increasing [C] to 8×10^{19} cm^{-3}. Figure 6(c) shows the S values at $E = 10$ keV for $Al_{0.1}Ga_{0.9}N$ with and without illumination. In the region of [C] $= 3 \times 10^{18}$–8×10^{19} cm^{-3}, the S values measured in the dark increased with increasing [C]; this trend is consistent with that of XRD measurement results. However, the S value for $Al_{0.1}Ga_{0.9}N$ with [C] $= 5 \times 10^{17}$ cm^{-3} was higher than that for $Al_{0.1}Ga_{0.9}N$ with [C] $= 3 \times 10^{18}$ cm^{-3}, which can be attributed to the suppression of the trapping of positrons by defects due to their charge transfers from neutral to positive and/or by the trapping of positrons by carbon atoms.

The localization of positrons near C_N was investigated by theoretical calculations. Figure 7 shows the projection of

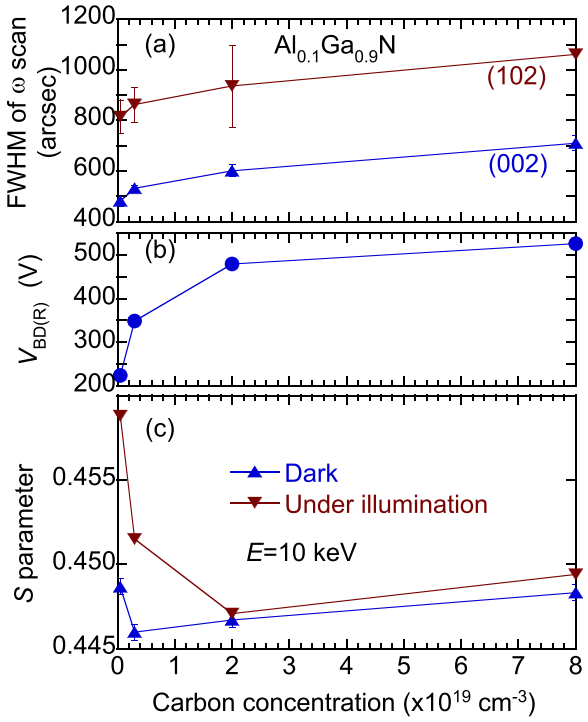

FIG. 6. (a) FWHM values of $Al_{0.1}Ga_{0.9}N$ (002) and (102) peaks obtained from XRD ω-rocking curves, (b) the breakdown voltage under reverse bias, $V_{BD(R)}$, and (c) the S values at $E = 10$ keV as a function of [C].

the positron densities near (a) C_N and (b) $(C_N)_4$ on the supercell ab-plane ($2\sqrt{3}\ a_0 \times 4\ a_0$), where the horizontal (x) and vertical (y) axes are parallel to the $[10\bar{1}0]$ and $[\bar{1}2\bar{1}0]$ axes of the wurtzite cell, respectively. The positron densities and the supercell were cut by the x-y plane at $z/c = 0.4$. In Fig. 7(b), the fourth carbon atom (not shown) locates above the center of three other carbon atoms. The colors on the cross section of the positron density represent the variations of the positron density, where the density increases following the sequence of "green → yellow → red." The charge state of the system was assumed to be neutral. The positron density distribution for $(C_N)_4$ is not a complete threefold symmetric, which is due to an artifact caused by the orthorhombic supercell used in the simulation and does not influence the

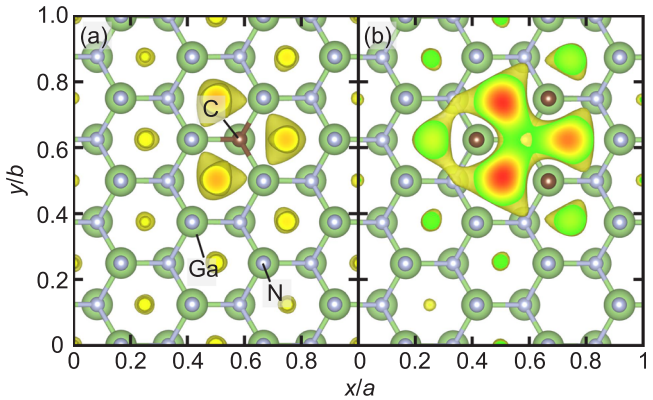

FIG. 7. Distributions of the positron density around (a) C_N and (b) $(C_N)_4$. Green, gray, and brown circles correspond to Ga, N, and C, respectively. The positron density increases following the color scale as "green → yellow → red."

conclusion. It can be seen that a positron tends to accumulate near C_N, suggesting that C_N is the shallow trapping center of positrons. The bond distance between C and Ga was almost identical to that between N and Ga (0.195 nm). Thus, the major reason of the positron density modulation is the charge re-distribution of atoms near C_N. A further localization of positrons near C_N occurred for $(C_N)_4$. The (S,W) values for C_N and $(C_N)_4$ were calculated, but they were almost identical to (S,W) for DF.

Figure 8 shows the distributions of the positron density averaged in the *ab*-plane, and the difference, between the positron densities for C_N-related defects and DF-GaN, $\Delta\rho_+$. Here, $\Delta\rho_+$ equals the positron density for a particular defect minus that for the DF-GaN. The result for V_{Ga} is also shown. The modulation of the positron density by C-related defects is an order of magnitude smaller than that by V_{Ga}. However, when [C] is one or two orders higher than the concentration of vacancy-type defects, the C-related defects could play a dominant role over the vacancy-type defects in positron trapping.

Using hybrid functional calculation, Lyons *et al.*[13] suggested that the absorption corresponding to transition of C_N^- to C_N^0 occurs at 2.95 eV with an onset energy at 2.60 eV. This agrees with the energy range corresponding to the increase in S (2.7−3.2 eV in Fig. 5). For $Al_{0.1}Ga_{0.9}N$ with $[C] = 5 \times 10^{17}\,cm^{-3}$, therefore, if the small S value observed in dark is due to the localization of positrons near C_N and the resultant suppression of the trapping of positrons by vacancies, this reaction ($C_N^- \rightarrow C_N^0 + e^-$) would partially be an origin of the observed optical response of S. As discussed above, however, when $[C_N]$ is close to the concentration of neutral vacancies, positrons are preferentially trapped by the vacancy-type defects. Thus, taking into account of C_N in the charge transfer of the vacancy-type defects, a possible reaction that could explain the behavior of S is $C_N^- + V^+ \rightarrow C_N^0 + V^0$.

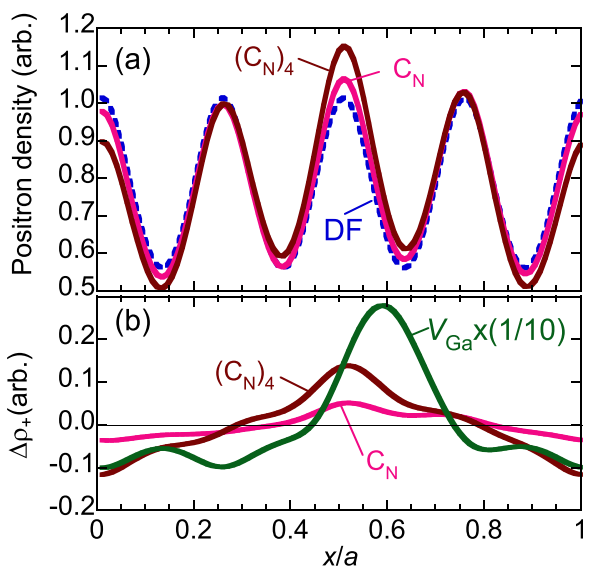

FIG. 8. (a) Planar averaged positron densities for C_N, $(C_N)_4$, and DF-GaN. The differences between the positron densities for C_N-related defects and DF-GaN, $\Delta\rho_+$, are shown in (b), where the results for V_{Ga} (multiplied by 1/10) are also shown.

As shown in Fig. 6(c), the effect of illumination on S was suppressed with increasing [C], suggesting the suppression of the electron capture by the vacancy-type defects. Thus, the C-related defects are considered to act as a scavenger of electrons emitted under illumination, and prevent the electron capture by the vacancies. Threading dislocations have been suggested to play a dominant role in the breakdown process of C-doped GaN.[8,11,49] The dislocations provide leakage current paths and electron transfer can occur via a trap-assisted tunneling processes.[50] According to Fig. 6(a), there should be a higher number of dislocations in the samples with increasing [C], while simultaneously the buffer leakage mechanism gradually deviated from a pure Poole-Frankel model. This suggested that other leakage mechanisms, which we speculate to be associated with dislocations, play a more dominant role over the Poole-Frankel mechanism. According to the concept of a Cottrell atmosphere,[51] the concentrations of the positively charged vacancies and/or C-related acceptors tend to increase around dislocation cores. Those defects can act as traps for those electrically injected electrons in the similar way as for those photoelectrons and could suppress the hopping probability of electrons along dislocations. This, thereby, increases the leakage blocking capability of the carbon-doped buffer as observed in this study.

IV. CONCLUSION

We used the positron annihilation spectroscopy to study vacancy-type defects in $Al_{0.1}Ga_{0.9}N$ layers grown on Si. The major vacancy species was determined to be a complex between V_{III} (or V_{III}s) coupled with V_Ns and/or with C_Ns. The charge state of the vacancies was determined to be positive in dark, and the trapping of emitted electrons by the defects changed their charge state from positive to neutral. The introduction of the positively charged vacancies was due to the electron transfer from the defects to C_N-related acceptors. The energy range of illumination which causes the charge transition of the defects agreed with yellow and blue luminescence bands, suggesting that those emission processes involved the interaction between emitted electrons and the vacancy-type defects.

With increasing [C] in $Al_{0.1}Ga_{0.9}N$, the breakdown voltage under reverse bias increased. For the samples with high [C], the illumination effect on the defect charge was diminished, which was attributed to the electron capture by C_N-related defects. Those results suggest that the positively charged defects and C_N-related acceptors play an important role in the suppression of leakage currents of $Al_{0.1}Ga_{0.9}N$. We have shown that positron annihilation parameters are sensitive to native vacancy-type defects in AlGaN grown on Si, and that positron annihilation spectroscopy is a useful tool for understanding the electric characteristics of buffer layers used for GaN-based power devices.

[1]S. W. Kaun, M. H. Wong, U. K. Mishra, and J. S. Speck, Semicond. Sci. Technol. **28**, 074001 (2013).
[2]B. J. Baliga, Semicond. Sci. Technol. **28**, 074011 (2013).
[3]K. Cheng, H. Liang, M. Van Hove, K. Geens, B. De Jaeger, P. Srivastava, X. W. Kang, P. Favia, H. Bender, S. Decou-tere, J. Dekoster, J. I. del Agua Borniquel, S. W. Jun, and H. Chung, Appl. Phys. Express **5**, 011002 (2012).

[4]M. Van Hove, S. Boulay, S. R. Bahl, S. Stoffels, X. W. Kang, D. Wellekens, K. Geens, A. Delabie, and S. Decou-tere, IEEE Electron Device Lett. **33**, 667 (2012).
[5]S. Lenci, B. De Jaeger, L. Carbonell, J. Hu, G. Mannaert, D. Wellekens, S. You, B. Bakeroot, and S. Decoutere, IEEE Electron Device Lett. **34**, 1035 (2013).
[6]M. Zhao, Y. Saripalli, P. K. Kandaswamy, H. Liang, A. Firrincieli, S. Decoutere, and E. Vancoille, Phys. Status Solidi C **11**, 446 (2014).
[7]C. Poblenz, P. Waltereit, S. Rajan, S. Heikman, U. K. Mishra, and J. S. Speck, J. Vac. Sci. Technol. B **22**, 1145 (2004).
[8]M. J. Uren, M. Cäsar, M. A. Gajda, and M. Kuball, Appl. Phys. Lett. **104**, 263505 (2014).
[9]X. Li, D. Zhao, D. Jiang, P. Chen, J. Zhu, Z. Liu, L. Le, J. Yang, and X. He, J. Vac. Sci. Technol. B **34**, 011204 (2015).
[10]M. Huber, I. Daumiller, A. Andreev, M. Silvestri, L. Knuuttila, A. Lundskog, M. Wahl, M. Kopnarski, and A. Bonanni, J. Appl. Phys. **119**, 125701 (2016).
[11]H. Yacoub, D. Fahle, M. Eickelkamp, A. Wille, C. Mauder, M. Heuken, H. Kalisch, and A. Vescan, J. Appl. Phys. **119**, 135704 (2016).
[12]J. Hu, S. Stoffels, S. Lenci, G. Groeseneken, and S. Decoutere, IEEE Electron Device Lett. **37**, 310 (2016).
[13]J. L. Lyons, A. Janotti, and C. G. Van de Walle, Appl. Phys. Lett. **97**, 152108 (2010).
[14]D. O. Demchenko, I. C. Diallo, and M. A. Reshchikov, Phys. Rev. Lett. **110**, 087404 (2013).
[15]S. Stoffels, M. Zhao, R. Venegas, P. Kandaswamy, S. You, T. Novak, Y. Saripalli, M. Van Hove, and S. Decoutere, in Proceedings of the IEEE International Electron Devices Meeting (2015), p. 35.4.1.
[16]R. Krause-Rehberg and H. S. Leipner, *Positron Annihilation in Semiconductors*, Solid-State Sciences (Springer-Verlag, Berlin, 1999), Vol. 127.
[17]F. Tuomisto and I. Makkonen, Rev. Mod. Phys. **85**, 1583 (2013).
[18]K. Saarinen, T. Suski, I. Grzegory, and D. C. Look, Physica B **308**, 77 (2001).
[19]A. Uedono, S. F. Chichibu, Z. Q. Chen, M. Sumiya, R. Suzuki, T. Ohdaira, T. Mikado, T. Mukai, and S. Nakamura, J. Appl. Phys. **90**, 181 (2001).
[20]O. Moutanabbir, R. Scholz, S. Senz, U. Gösele, M. Chicoine, F. Schiettekatte, F. Süßkraut, and R. Krause-Rehberg, Appl. Phys. Lett. **93**, 031916 (2008).
[21]M. J. Wang, L. Yuan, C. C. Cheng, C. D. Beling, and K. J. Chen, Appl. Phys. Lett. **94**, 061910 (2009).
[22]S. Hautakangas, K. Saarinen, L. Liszkay, J. A. Freitas, Jr., and R. L. Henry, Phys. Rev. B **72**, 165303 (2005).
[23]J. Xu, Q. Li, W. Zhang, J. Liu, H. Du, and B. Ye, Chem. Phys. Lett. **616–617**, 161 (2014).
[24]X. F. Li, Z. Q. Chen, C. Liu, H. J. Zhang, and A. Kawasuso, J. Appl. Phys. **117**, 085706 (2015).
[25]M. Zhao, H. Liang, P. K. Kandaswamy, M. Van Hove, R. Venegas, E. Vranken, P. Favia, A. Vanderheyden, D. Vanhaeren, Y. N. Saripalli, S. Decoutere, and R. Langer, Phys. Status Solidi C **13**, 311 (2016).
[26]A. van Veen, H. Schut, M. Clement, J. M. M. de Nijs, A. Kruseman, and M. R. Ijpma, Appl. Surf. Sci. **85**, 216 (1995).
[27]A. Uedono, S. Ishibashi, N. Oshima, and R. Suzuki, Jpn. J. Appl. Phys., Part 1 **52**, 08JJ02 (2013).
[28]S. Ishibashi, T. Tamura, S. Tanaka, M. Kohyama, and K. Terakura, Phys. Rev. B **76**, 153310 (2007).
[29]P. E. Blöchl, Phys. Rev. B **50**, 17953 (1994).
[30]J. P. Perdew, K. Burke, and M. Ernzerhof, Phys. Rev. Lett. **77**, 3865 (1996).
[31]E. Boroński and R. M. Nieminen, Phys. Rev. B **34**, 3820 (1986).
[32]M. J. Puska, S. Mäkinen, M. Manninen, and R. M. Nieminen, Phys. Rev. B **39**, 7666 (1989).
[33]S. Ishibashi and A. Uedono, J. Phys.: Conf. Ser. **674**, 012009 (2014).
[34]A. Zunger, S.-H. Wei, L. G. Ferreira, and J. E. Bernard, Phys. Rev. Lett. **65**, 353 (1990).
[35]C. Zhou, Q. Jiang, S. Huang, and K. J. Chen, in Proceedings of the International Symposium on Power Semiconductor Devices & ICs (2012), p. 245.
[36]Z. Chunhua, J. Qimeng, H. Sen, and K. J. Chen, IEEE Electron Device Lett. **33**, 1132 (2012).
[37]M. A. Lampert, Phys. Rev. **103**, 1648 (1956).
[38]A. Rizzo, G. Micocci, and A. Tepore, J. Appl. Phys. **48**, 3415 (1977).
[39]A. Pérez-Tomás, A. Fontserè, J. Llobet, M. Placidi, S. Rennesson, N. Baron, S. Chenot, J. C. Moreno, and Y. Cordier, J. Appl. Phys. **113**, 174501 (2013).
[40]H. Yacoub, D. Fahle, M. Finken, H. Hahn, C. Blumberg, W. Prost, H. Kalisch, M. Heuken, and A. Vescan, Semicond. Sci. Technol. **29**, 115012 (2014).
[41]A. Uedono, Y. Tsukada, Y. Mikawa, T. Mochizuki, H. Fujisawa, H. Ikeda, K. Kurihara, K. Fujito, S. Terada, S. Ishibashi, and S. F. Chichibu, J. Cryst. Growth **448**, 117 (2016).
[42]A. Uedono, S. Ishibashi, K. Tenjinbayashi, T. Tsutsui, K. Nakahara, D. Takamizu, and S. F. Chichibu, J. Appl. Phys. **111**, 014508 (2012).
[43]A. Uedono, T. Fujishima, Y. Cao, Y. Zhang, N. Yoshihara, S. Ishibashi, M. Sumiya, O. Laboutin, W. Johnson, and T. Palacios, Appl. Phys. Lett. **104**, 082110 (2014).
[44]A. Uedono, T. Fujishima, D. Piedra, N. Yoshihara, S. Ishibashi, M. Sumiya, O. Laboutin, W. Johnson, and T. Palacios, Appl. Phys. Lett. **105**, 052108 (2014).
[45]S. R. Lee, A. F. Wright, M. H. Crawford, G. A. Petersen, J. Han, and R. M. Biefeld, Appl. Phys. Lett. **74**, 3344 (1999).
[46]M. A. Reshchikov and H. Morkoç, J. Appl. Phys. **97**, 061301 (2005).
[47]A. Y. Polyakov, M. Shin, J. A. Freitas, Jr., M. Skowronski, D. W. Greve, and R. G. Wilson, J. Appl. Phys. **80**, 6349 (1996).
[48]C. H. Seager, A. F. Wright, J. Yu, and W. Götz, J. Appl. Phys. **92**, 6553 (2002).
[49]Y. Zhang, M. Sun, H.-Y. Wong, Y. Lin, P. Srivastava, C. Hatem, M. Azize, D. Piedra, L. Yu, T. Sumitomo, N. de Almeida Braga, V. Mickevicius, and T. Palacios, IEEE Trans. Electron Devices **62**, 2155 (2015).
[50]E. J. Miller, E. T. Yu, P. Waltereit, and J. S. Speck, Appl. Phys. Lett. **84**, 535 (2004).
[51]A. H. Cottrell and B. A. Bilby, Proc. Phys. Soc. **62A**, 49 (1949).